Progress In Electromagnetics Research M, Vol. 104, 81–89, 2021

Electromagnetic Properties of a Babinet-Type Metasurface Composed of Coaxial-Sector Apertures

Alexandr V. Gribovsky[1, 2], Yuliia V. Antonenko[1, 2], Yevhenii O. Antonenko[1, *], and Victor A. Katrich[1]

Abstract—Electromagnetic properties of a planar metallic metasurface with the design inspired by Babinet's principle are numerically studied. The metasurface is constructed from a metal plate perforated by coaxial-sector apertures. It is shown that the chosen coaxial-sector apertures make it possible to obtain a wider operating range of the metasurface than those composed of apertures of other shapes (e.g., round or rectangle). Moreover, the proposed metasurface performs an efficient polarization conversion of the linearly polarized wave to elliptically and circularly polarized ones in the reflected field.

1. INTRODUCTION

Traditional planar metamaterials (metasurfaces) for microwave operating range are made of periodic arrays of complex-shaped sub-wavelength metallic particles aligned on a thin dielectric substrate, or according to Babinet's principle [1], they can be formed from a metallic plate perforated with apertures of a complicated shape [2–5]. Typically, the particles are symmetrical split-ring resonators, which act as a chain of LC-circuits resulting in a resonant interaction of electromagnetic waves with a patterned layer. Thereby, resonant planar metamaterials can, in a way, maintain an electromagnetic environment similar to those existing in traditional volumetric resonators (cavities) and thus be considered as their alternative in certain applications [6–19].

The overwhelming majority of current investigations, both theoretical and experimental, in the field of metamaterial deal with the designs that represent two-dimensional (2D) periodic microstrips, split-ring resonators [20–22], 2D multi-element dielectric structures [23, 24], or arrays of axial irises [25]. Primarily, metasurfaces are treated as optical devices in which the light is controlled through changing its phase, amplitude, frequency, polarization, and spatial structure.

Babinet-type metasurfaces made in the form of perforated metal screens are usually considered for their use as frequency-selective surfaces and filters [26]. Among Babinet-type metasurfaces, structures made in the form of a plate with coaxial-sector apertures demonstrate several advantages as compared with the metasurfaces comprising apertures of other geometries, for example, those with circular or rectangular holes. In particular, for the metasurfaces having the same spatial period, structures with the coaxial-sector geometry of holes can operate in a wider frequency range without appearance of higher-order diffraction beams in free space [27]. This follows from the fact that the cutoff wavelength of the coaxial-sector waveguides can exceed the respective values of circular and rectangular waveguides by a factor of 2 or 3. Moreover, metasurfaces composed of coaxial-sector apertures can operate in a multimode regime providing an efficient polarization conversion [28].

Received 13 June 2021, Accepted 13 August 2021, Scheduled 18 August 2021

* Corresponding author: Yevhenii O. Antonenko (antonenko@karazin.ua).

[1] Department of Radiophysics, Biomedical Electronics and Computer Systems, V. N. Karazin Kharkiv National University, 4, Svobody Sq., Kharkiv 61022, Ukraine. [2] Theoretical Radiophysics Department, Institute of Radio Astronomy of the National Academy of Sciences of Ukraine, 4, Mystetstv St., Kharkiv 61002, Ukraine.

In the present paper, the frequency-selective and polarization properties of a Babinet-type metasurface composed of coaxial-sector apertures are studied in detail with the use of the integrated numerical algorithm formulated for the generalized scattering matrices of a 2D array of semi-infinite coaxial-sector waveguides [29].

2. GENERAL STATEMENTS

In what follows, two particular designs of the metasurface are under consideration. The metasurface of the first kind represents a perfectly conducting plate of a finite thickness perforated by "coaxial-rib" apertures (Fig. 1(a)), whereas the metasurface of the second kind is a plate with "coaxial-comb" apertures (Fig. 1(b)). A schematic view of the unit cell of the metasurface under study is illustrated in Fig. 2. We consider that the metasurface is illuminated by a normally incident plane either TE- or TM-wave.

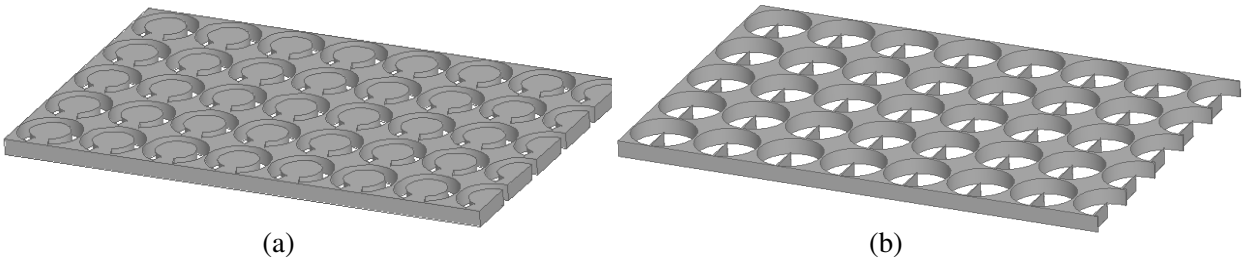

Figure 1. Metasurface with (a) coaxial-rib and (b) coaxial-comb apertures.

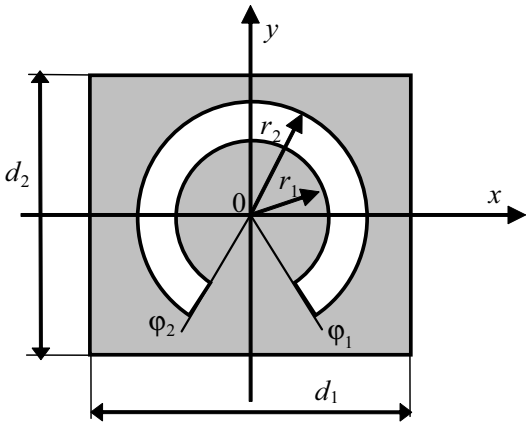

Figure 2. Coordinate frame and schematic view of the unit cell of the metasurface under study.

Under such irradiation conditions, various modes of the coaxial-sector apertures (waveguides) can be excited. In our study, only several lowest-order modes are important. The electric field distributions across transverse sections of coaxial-rib and coaxial-comb waveguides at the propagation frequencies for three lowest-order waveguide modes are presented in Figs. 3 and 4, respectively (here $F_{cut}(TE_{mn})$ is the cutoff frequency of the TE_{mn} waveguide mode).

We should note that the wavelength λ of the higher-order propagating waveguide modes in the multimode regime remains greater than the structure period (the subwavelength conditions). This allows the proposed metasurfaces to operate in a wide frequency range without the appearance of higher-order diffraction beams in free space.

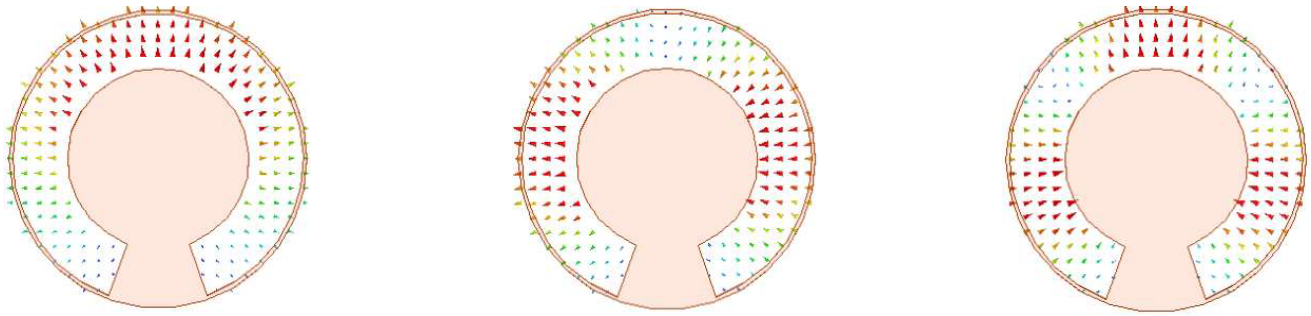

Figure 3. Electric field distribution in a cross-section of the coaxial-rib waveguide for (a) TE_{11}-mode, $f = 9\,\text{GHz}$ ($F_{cut}(TE_{11}) = 8.327\,\text{GHz}$), (b) TE_{21}-mode, $f = 17\,\text{GHz}$ ($F_{cut}(TE_{21}) = 16.641\,\text{GHz}$), and (c) TE_{31}-mode, $f = 27\,\text{GHz}$ ($F_{cut}(TE_{31}) = 24.93\,\text{GHz}$). Parameters of the waveguide are: $r_1 = 2.5\,\text{mm}$, $r_2 = 4\,\text{mm}$, $\varphi_1 = -0.39\pi$, $\varphi_2 = 1.39\pi$, and $d_1 = d_2 = 9\,\text{mm}$.

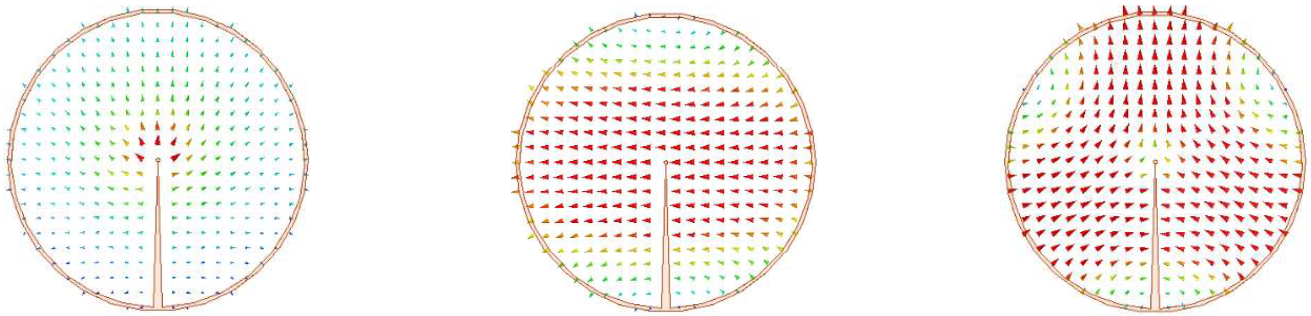

Figure 4. Electric field distribution in a cross-section of the coaxial-comb waveguide for (a) TE_{11}-mode, $f = 14\,\text{GHz}$, ($F_{cut}(TE_{11}) = 13.7597\,\text{GHz}$), (b) TE_{21}-mode, $f = 23\,\text{GHz}$ ($F_{cut}(TE_{21}) = 22.126\,\text{GHz}$), (c) TE_{31}-mode, $f = 30\,\text{GHz}$ ($F_{cut}(TE_{31}) = 29.589\,\text{GHz}$). Parameters of the waveguide are: $r_1 = 0.05\,\text{mm}$, $r_2 = 4\,\text{mm}$, $\phi_1 = -0.49\pi$, $\phi_2 = 1.49\pi$, and $d_1 = d_2 = 9\,\text{mm}$.

3. FREQUENCY-SELECTIVE TRANSMISSION

In this section, the spectral characteristics of the reflection coefficient magnitude are analyzed for different geometric parameters of the metasurface. Spatial orientations of the electromagnetic field vectors of the incident TE- and TM-waves are shown in Fig. 5, where θ and ϕ are the angles of plane wave incidence in the spherical coordinates, and α is the azimuth angle which specifies the orientation of the polarization vector of the incident wave. This angle is equal to $\alpha = 0°(180°)$ for the TE-wave and $\alpha = 90°(-90°)$ for the TM-wave, respectively. Under the normal incidence conditions ($\theta = 0°$ and $\phi = 0°$) the electric field vector $\vec{E}$ of the TE- and TM-waves is oriented along the y- and x-axes, respectively.

The results of simulation of the frequency-selective properties of the metasurface made of a plate perforated by the coaxial-rib and coaxial-comb apertures are summarized in Figs. 6 and 7, respectively. In these figures, the points depicted on the frequency scale indicate the cutoff frequencies of three lowest-order waveguide modes. One can conclude that the selective excitation of the modes of coaxial-rib waveguides occurs when the metasurface is irradiated with waves of orthogonal polarization, and as the thickness of the plate increases, additional resonances of the total transmission appear in the metasurface spectra in the chosen frequency band.

In particular, the selective excitation manifests itself in the fact that when the metasurface is irradiated with the TE-wave, the resonances arise in the range of the TE_{11} and TE_{31} waveguide modes

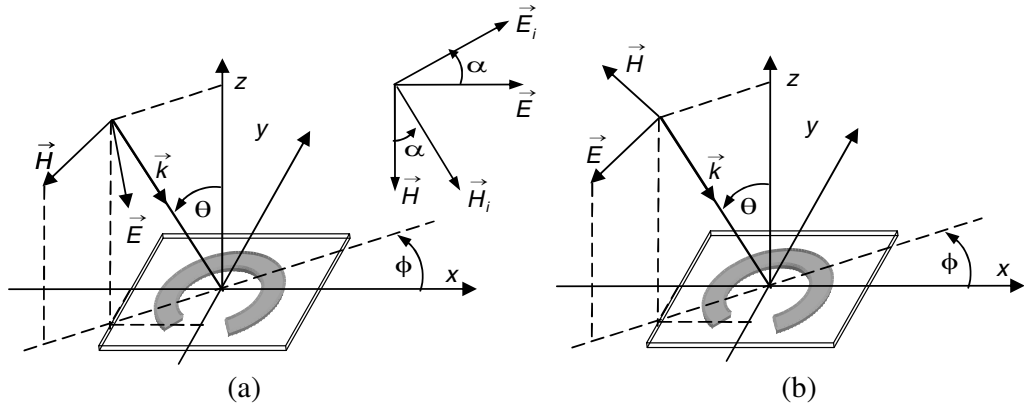

Figure 5. Spatial orientation of the electromagnetic field vectors of the plane linearly polarized (a) TE-wave and (b) TM-wave.

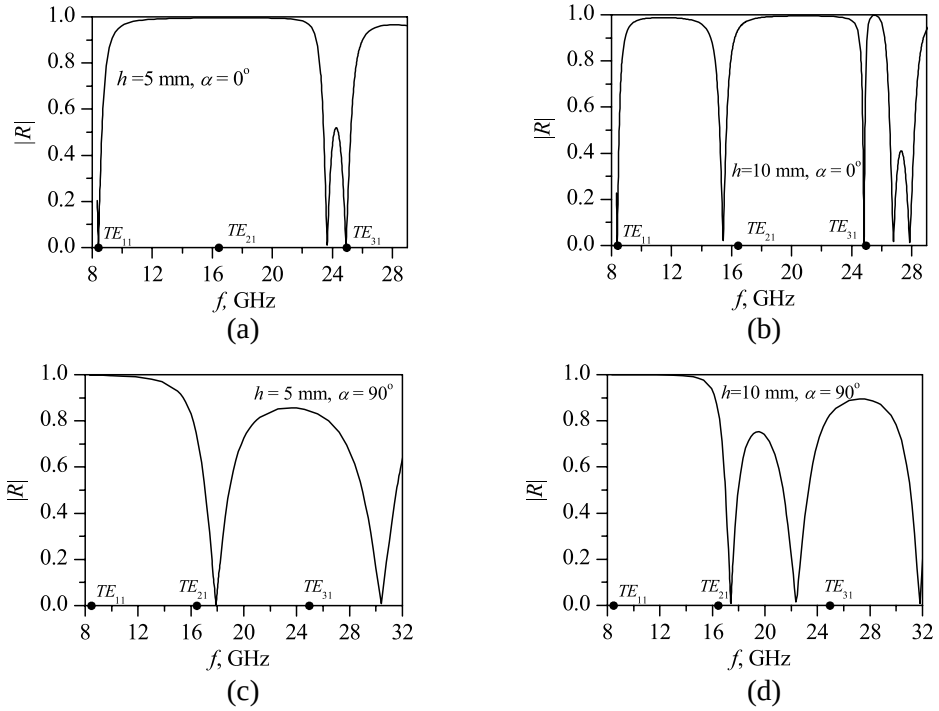

Figure 6. Reflection coefficient magnitude of the metasurface made of a plate with thickness $h = 5\,\text{mm}$ and $h = 10\,\text{mm}$ perforated by coaxial-rib apertures. The metasurface is excited by (a), (b) TE-wave, and (c), (d) TM-wave.

(Figs. 6(a) and 6(b)), whereas for the TM wave, they are in the frequency range of the TE_{21} waveguide mode propagation (Figs. 6(c) and 6(d)). This effect is explained by the presence of the corresponding components of the electric field vector in the coaxial-rib waveguide mode providing their coupling with the field of the incident wave (see Fig. 3(a) and Fig. 3(b)).

In addition, Figs. 6(a) and 6(b) demonstrate the appearance of stopbands, whose central frequencies and widths are dependent on both the metasurface thickness and polarization of the incident wave. These stopbands can be used, for example, for electromagnetic wave filtering.

The reflection coefficient magnitude of the metasurface made of a plate perforated by the coaxial-comb apertures is presented in Fig. 7 for two different metasurface thicknesses and orthogonal polarizations of the incident wave. The characteristic size of the metasurface unit cell is fixed as in the previous case.

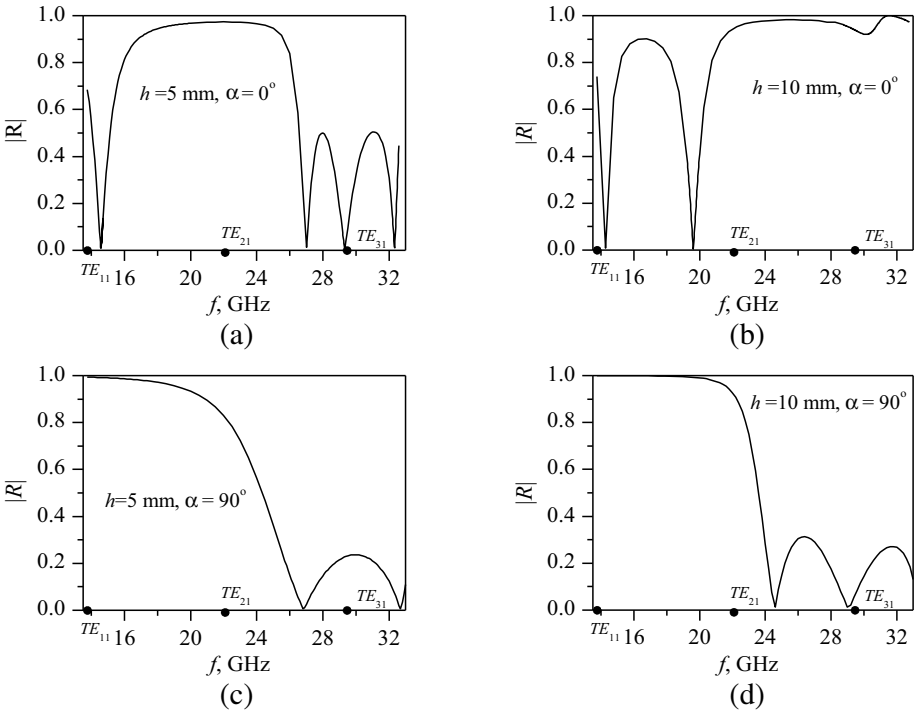

Figure 7. Same as in Fig. 6 but for the metasurface composed of coaxial-comb apertures.

Similar to the metasurface of the first kind, the resonant frequencies of the total transmission for the metasurface with coaxial-comb apertures are dependent on the orientation of the field polarization vector of the incident wave and the present components of the electric field vector of the mode of the coaxial-comb waveguides. However, the number of these resonances in the selected frequency range changes in different ways as the metasurface thickness changes, depending on the excitation mode. Thus, with thickening the plate, the number of resonances of the total transmission increases in the case of the metasurface excitation by the TE-wave and decreases for the TM-wave. The stopbands appear also in the spectra of the metasurface of the second kind. As can be seen, characteristics of these bands are dependent on both the metasurface thickness and polarization of the incident wave.

4. POLARIZATION CONVERSION

In this section, we study the ability of the given metasurface to perform polarization transformation of normally incident TE and TM waves. Polarization state of the incident wave is defined by the value of the azimuth angle α, which determines the orientation of the vector E on the x-y plane. The intensity of the diffracted electromagnetic field $|R|^2$ is calculated according to the equation $|R|^2 = |R_{TE}^2 + |R_{TM}^2$, where $|R_{TE}|$ and $|R_{TM}|$ are the amplitudes of the reflected TE- and TM-waves, respectively.

The polarization characteristics of the reflected field of the metasurface with coaxial-rib apertures are presented in Fig. 8 for three different frequencies of the incident wave.

As can be seen from the dependences presented in Fig. 8, the coaxial-rib apertures support propagation of two waveguide modes, specifically TE_{11} and TE_{21} at the frequency of 20 GHz, whose electric field vectors in the waveguide cross-section are mutually orthogonal. With a non-zero direction angle of the incident wave polarization vector, two waveguide modes, namely, TE_{11} and TE_{21}, are simultaneously excited in the waveguide channels. The curves $|R_{TE}(\alpha)|$ and $|R_{TM}(\alpha)|$ experience crossing at $\alpha = 55°$ where the magnitudes of the reflected TE and TM waves are identical. The phase difference between the reflected TE- and TM-waves in this case is approximately equal to 90°. Hence, the metasurface with the coaxial-rib apertures transforms the incident linearly polarized wave into a reflected wave with circular polarization. The polarization transformation efficiency is 72%. A

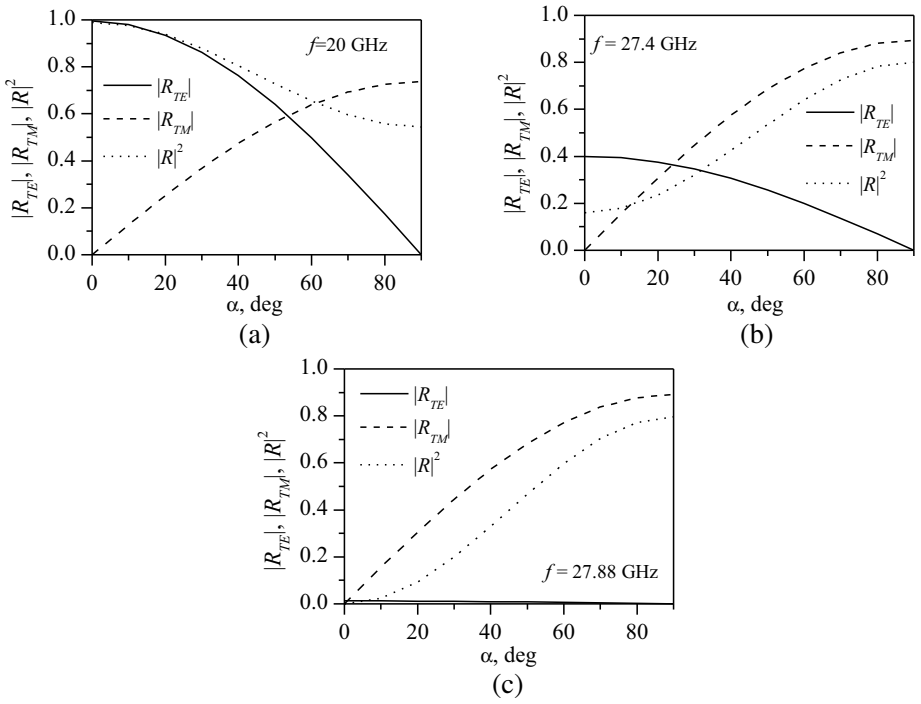

Figure 8. Reflected field magnitude as function of the azimuth angle α for the metasurface with coaxial-rib apertures irradiated with the wave at frequency of (a) $f = 20\,\mathrm{GHz}$, (b) $f = 27.4\,\mathrm{GHz}$, and (c) $f = 27.88\,\mathrm{GHz}$.

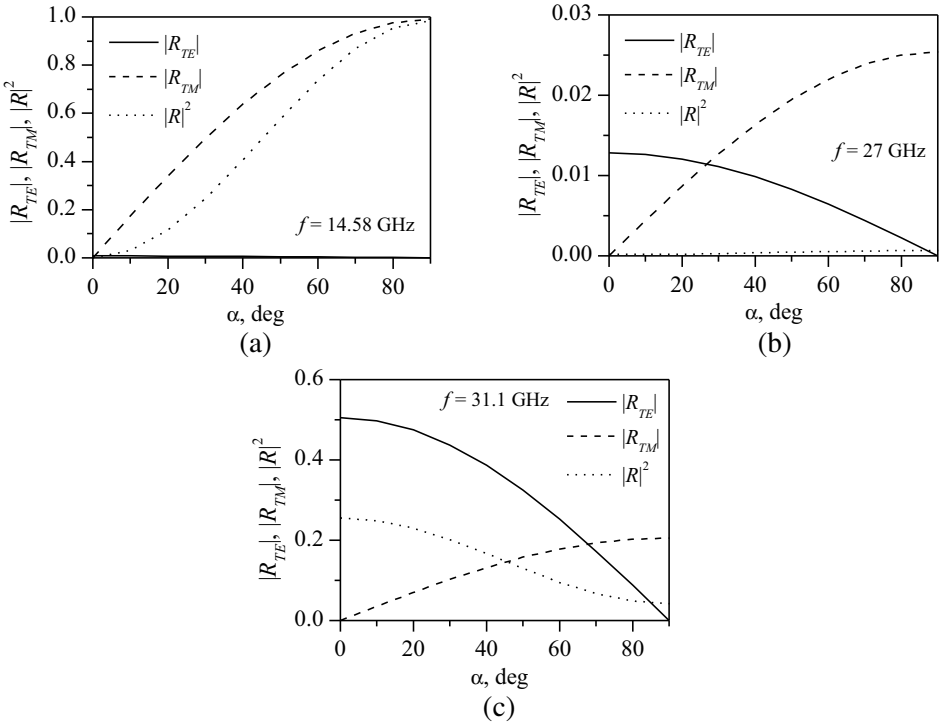

Figure 9. Reflected field magnitude as function of the azimuth angle α for the metasurface with coaxial-comb apertures irradiated with the wave at frequency of (a) $f = 14.58\,\mathrm{GHz}$, (b) $f = 27.0\,\mathrm{GHz}$, and (c) $f = 31.1\,\mathrm{GHz}$.

similar situation is observed at the frequency $f = 27.4\,\text{GHz}$ (see Fig. 8b) for the orientation angle of the incident field polarization vector equal to 25° in which polarization efficiency is 25%. At the frequency $f = 27.88\,\text{GHz}$, the coaxial-rib apertures support simultaneous propagation of three waveguide modes. As follows from Fig. 8(c), polarization of the reflected field is independent of the polarization of the incident wave. The metasurface reflects the electromagnetic TM-wave whose electric field vector is directed along the x-axis throughout the variation range of the incident wave polarization.

The corresponding curves related to polarization characteristics of the metasurface with coaxial-comb apertures are summarized in Fig. 9.

At the frequency $f = 14.58\,\text{GHz}$, polarization of the wave reflected from the metasurface is independent of the incident wave polarization and remains unchanged throughout the variation range of the azimuth angle of the incident wave. At that, the power reflection factor changes from 0 to 1. The polarization efficiencies for the frequencies $f = 27.0\,\text{GHz}$ and $f = 31.1\,\text{GHz}$ are practically independent of the incident wave polarization, and the metasurface with coaxial-rib apertures proves to be either completely or partially transparent for the incident wave throughout the variation range of the polarization vector orientation of the incident wave.

5. CONCLUSION

In the paper, frequency-selective and polarization properties are analyzed for the metasurfaces of two kinds. They represent a perfectly conducting plate perforated by either "coaxial-rib" or "coaxial-comb" apertures. The given metasurfaces are capable to operate in a wider frequency range as compared against similar metasurfaces with apertures of other geometries. This is explained by the unique capability of the coaxial-sector apertures to operate in the multimode regime without appearance of higher-order diffraction beams in free space. It has been found that in the metasurface spectra several stop bands appear. Parameters of these stopbands are dependent on the metasurface thickness and polarization of the incident wave. An analysis of the polarization properties of the metasurfaces has shown that the metasurface under study is capable to transform the incident wave with linear polarization into a reflected wave with elliptical polarization which can be approached to the circular one. Moreover, the metasurface is transparent for the wave with specific polarization. The polarization efficiency of the metasurface is independent of the polarization of the incident wave.

Thus, based on the obtained results it can be concluded that the proposed metasurface can be applied in various devices and units. In particular, it can be used inside and outside the resonator devices for formation of electromagnetic beams with certain polarization properties [30]. To check the basic electromagnetic properties of metal plates perforated with coaxial-sector apertures, preliminary experimental studies of the Fabry-Perot resonator were carried out [31]. Two classical technologies are well suited for the manufacture of experimental samples: milling technology and laser cutting. Laser cutting technology has the advantage of precision and can produce metasurfaces for use up to approximately 150 GHz.

REFERENCES

1. Falcone, F., T. Lopetegi, M. A. G. Laso, J. D. Baena, J. Bonache, M. Beruete, R. Marqués, F. Martín, and M. Sorolla, "Babinet principle applied to the design of metasurfaces and metamaterials," *Physical Review Letters*, Vol. 93, No. 19, 197401, 2004.
2. Berdnik, S. L., V. A. Katrich, and V. A. Lyaschenko, "Closely spaced transverse slots in rectangular waveguide," *Proceedings 4th International Conference on Antenna Theory and Techniques*, Sevastopol, Ukraine, September 9–12, 2003.
3. Tuz, V. R., S. L. Prosvirnin, and L. A. Kochetova, "Optical bistability involving planar metamaterials with broken structural symmetry," *Physical Review B*, Vol. 82, No. 23, 233402, 2010.
4. Khardikov, V., P. Mladyonov, S. Prosvirnin, and V. Tuz, "Electromagnetic wave diffraction by periodic planar metamaterials with nonlinear constituents," *Chapter 5 in Contemporary Optoelectronics, Springer Series in Optical Sciences*, 81–98, 2016.

5. Antonenko, Y. V., Ye. A. Antonenko, and A. V. Gribovsky, "Experimental investigation of frequency-selective properties of metal metasurface supporting a trapped mode resonance," *Proceedings Ukrainian Microwave Week*, Kharkiv, Ukraine, September 21–25, 2020.
6. Politano, G. G., E. Cazzanelli, C. Versace, C. Vena, M. P. De Santo, M. Castriota, F. Ciuchi, and R. Bartolino, "Graphene oxide on magnetron sputtered silver thin films for SERS and metamaterial applications," *Applied Surface Science*, Vol. 427, 927–933, 2018.
7. Sadhukhan, K., A. Politano, and A. Agarwal, "Novel undamped gapless plasmon mode in a tilted Type-II dirac semimetal," *Physical Review Letters*, Vol. 124, No. 4, 046803, 2020.
8. Chiarello, G., J. Hofmann, Z. Li, V. Fabio, L. Guo, X. Chen, S. Das Sarma, and A. Politano, "Tunable surface plasmons in Weyl semimetals TaAs and NbAs," *Physical Review B*, Vol. 99, No. 12, 121401, 2019.
9. Politano, A., G. Chiarello, B. Ghosh, K. Sadhukhan, C.-N. Kuo, C. S. Lue, V. Pellegrini, and A. Agarwal, "3D dirac plasmons in the Type-II dirac semimetal PtTe 2," *Physical Review Letters*, Vol. 121, No. 8, 086804, 2018.
10. Agarwal, A., M. S. Vitiello, L. Viti, A. Cupolillo, and A. Politano, "Plasmonics with two-dimensional semiconductors: From basic research to technological applications," *Nanoscale*, Vol. 10, No. 19, 8938–8946, 2018.
11. Politano, A. and G. Chiarello, "Plasmon modes in graphene: Status and prospect," *Nanoscale*, Vol. 6, No. 19, 10927–10940, 2014.
12. Viti, L., D. Coquillat, A. Politano, K. A. Kokh, Z. S. Aliev, M. B. Babanly, O. E. Tereshchenko, W. Knap, E. V. Chulkov, and M. S. Vitiello, "Plasma-wave terahertz detection mediated by topological insulators surface states," *Nano Letters*, Vol. 16, No. 1, 80–87, 2016.
13. Politano, A., L. Viti, and M. S. Vitiello, "Optoelectronic devices, plasmonics, and photonics with topological insulators," *APL Materials*, Vol. 5, No. 3, 035504, 2017.
14. Mitrofanov, O., L. Viti, E. Dardanis, M. C. Giordano, D. Ercolani, A. Politano, L. Sorba, and M. S. Vitiello, "Near-field terahertz probes with room-temperature nanodetectors for subwavelength resolution imaging," *Scientific Reports*, Vol. 7, No. 1, 1–10, 2017.
15. Zhang, L., Z. Chen, K. Zhang, L. Wang, H. Xu, L. Han, W. Guo, Y. Yang, C.-N. Kuo, C. S. Lue, D. Mondal, J. Fuji, I. Vobornik, B. Ghosh, A. Agarwal, H. Xing, X. Chen, X. Chen, and W. Lu, "High-frequency rectifiers based on Type-II dirac fermions," *Nature Communications*, Vol. 12, No. 1, 1–8, 2021.
16. Guo, C., Y. Hu, G. Chen, D. Wei, L. Zhang, Z. Chen, W. Guo, H. Xu, C.-N. Kuo, C. S. Lue, X. Bo, X. Wan, L. Wang, X. Chen, X. Chen, and W. Lu, "Anisotropic ultrasensitive PdTe2-based phototransistor for room-temperature long-wavelength detection," *Science Advances*, Vol. 6, No. 36, 2020.
17. Xu, H., C. Guo, J. Zhang, W. Guo, C.-N. Kuo, C. S. Lue, W. Hu, L. Wang, G. Chen, A. Politano, X. Chen, and W. Lu, "PtTe2-based Type-II dirac semimetal and its Van der Waals heterostructure for sensitive room temperature terahertz photodetection," *Small*, Vol. 15, No. 52, 1903362, 2019.
18. Tang, W., A. Politano, C. Guo, W. Guo, C. Liu, L. Wang, X. Chen, and W. Lu, "Ultrasensitive room-temperature terahertz direct detection based on a bismuth selenide topological insulator," *Advanced Functional Materials*, Vol. 28, No. 31, 1801786, 2018.
19. Chen, Y., A. S. Schwanecke, V. A. Fedotov, V. V. Khardikov, P. L. Mladyonov, S. L. Prosvirnin, A. V. Rogacheva, N. I. Zheludev, and E. Huq, "Electron beam lithography for high density meta fish scale operational at optical frequency," *Microelectronic Engineering*, Vol. 86, Nos. 4–6, 1081–1084, 2009.
20. Fedotov, V. A., M. Rose, S. L. Prosvirnin, N. Papasimakis, and N. I. Zheludev, "Sharp trapped-mode resonances in planar metamaterials with a broken structural symmetry," *Physical Review Letters PRL*, Vol. 99, 147401, 2007.
21. Alibakhshikenari, M., B. S. Virdee, P. Shukla, C. H. See, R. A. Abd-Alhameed, F. J. Falcone, and E. Limiti, "Meta-surface wall suppression of mutual coupling between microstrip patch antenna arrays for THz-band applications," *Progress In Electromagnetics Research Letters*, Vol. 75, 105–111, 2018.

22. Wang, S., P. C. Wu, V. C. Su, Y. C. Lai, C. H. Chu, J. W. Chen, and T. Li, "Broadband achromatic optical metasurface devices," *Nature Communications*, Vol. 8, No. 1, 1–9, 2017.
23. Prosvirnin, S. L., V. A. Dmitriev, Y. A. Kuleshov, and V. V. Khardikov, "Planar all-silicon metamaterial for terahertz applications," *Applied Optics*, Vol. 54, No. 13, 3986–3990, 2015.
24. Tuz, V. R., V. V. Khardikov, A. S. Kupriianov, K. L. Domina, S. Xu, H. Wang, and H.-B. Sun, "High-quality trapped modes in all-dielectric metamaterials," *Optics Express*, Vol. 26, No. 3, 2905–2916, 2018.
25. Legenkiy, M., "Analysis of axially symmetric diffraction grating," *Proceedings XI International Conference on Antenna Theory and Techniques (ICATT)*, Kyiv, Ukraine, May 24–27, 2017.
26. Wang, Y., B. Yang, Y. Tian, R. S. Donnan, and M. J. Lancaster, "Micromachined thick mesh filters for millimeter-wave and terahertz applications," *IEEE Trans. Terahertz Science and Technology*, Vol. 4, No. 2, 247–253, 2014.
27. Antonenko, Y. V. and A. V. Gribovsky, "Frequency-selective properties of a plane screen of finite thickness with coaxial-sector apertures," *Radio Physics and Radio Astronomy*, Vol. 2, No. 1, 77–83, 2011.
28. Antonenko, J. V. and A. V. Gribovsky, "Polarization transformation of electromagnetic waves on a reflector array of the short-circuited coaxial-sector waveguides," *Proceedings 13-th International Conference on Mathematical Methods in Electromagnetic Theory*, Kyiv, Ukraine, September 6–8, 2010.
29. Antonenko, J. V. and A. V. Gribovsky, "Frequency-selective properties of the flat screen of a finite thickness with coaxial-sectors apertures," *Proceedings International Kharkov Simposium on Physics and Engineering of Microwaves, Millimeter and Submillimeter Waves*, Kharkiv, Ukraine, June 21–26, 2010.
30. Cui, J., M. Legenkiy, V. Khrychov, S. Shulga, Z. Sun, and Y. Zheng, "Diffraction properties of azimuthally symmetric gratings in a hollow circular dielectric waveguide," *Results in Physics*, Vol. 18, 103204, 2020.
31. Antonenko, Y. V., Ye. A. Antonenko, and A. V. Gribovsky, "Experimental studies of the Fabry-Perot resonator with mirrors perforated by coaxial-sector holes," *Proceedings XXIVth International Seminar/Workshop on Direct and Inverse Problems of Electromagnetic and Acoustic Wave Theory (DIPED)*, Lviv, Ukraine, September 12–14, 2019.